

VELOCITY MEASUREMENTS OF HYDROGEN JETS USING THE OPTICAL FLOW METHOD

Huang, T.¹, Zhang, X.², Ba, Q.X.³, Zhao, M.B.⁴, Zhao, Z.Y.⁵, Christopher, D.M.^{6,*}, Li, X.F.^{7,*}

¹ Institute of Thermal Science and Technology, Shandong University, Jingshi Road, Jinan 250061, China, huang-teng@outlook.com

² Institute of Thermal Science and Technology, Shandong University, Jingshi Road, Jinan 250061, China, z xu9687@outlook.com

³ Institute of Thermal Science and Technology, Shandong University, Jingshi Road, Jinan 250061, China, qingxin90113@126.com

⁴ Institute of Thermal Science and Technology, Shandong University, Jingshi Road, Jinan 250061, China, zmb2018@mail.sdu.edu.cn

⁵ Institute of Thermal Science and Technology, Shandong University, Jingshi Road, Jinan 250061, China, zhao-zeying@outlook.com

⁶ Key Laboratory of Thermal Science and Power Engineering of Ministry of Education, Tsinghua University, Shuangqing Road, Beijing 100084, China, dmc@tsinghua.edu.cn

⁷ Institute of Thermal Science and Technology, Shandong University, Jingshi Road, Jinan 250061, China, lixf@email.sdu.edu.cn

ABSTRACT

Concentration and velocity measurements are crucial for developing and validating hydrogen jet models, which provide scientific bases for hydrogen safety analyses. The concentration fields have been visualized and accurately measured using laser diagnostic methods based on laser Rayleigh and Raman scattering techniques. However, the velocity measurements are more challenging. Particle image velocimetry (PIV) has been commonly used for measuring velocities in turbulent flows by seeding tracer particles into the flow and assuming the particles intimately following the flow. However, sometimes the particle seeding is difficult or disturbs the flow. Moreover, simultaneously concentration and velocity measurements are very difficult when using PIV systems to measure the velocities. Therefore, the optical flow velocimetry (OFV) method was used to resolve the velocity fields from the scalar fields or particle images of hydrogen jets. In the present work, the velocity field and particle images of hydrogen jets were simulated using FLUENT with the large eddy simulation (LES) model and the particle images were then used to resolve the velocity field by the OFV method. The OFV results were compared with the CFD simulations to verify their accuracy. The results show that the OFV method was an efficient, low-cost way to extract the velocity fields from particle images. The OFV method accurately located the large vortices in the flow and the velocity distribution of the high-velocity gradients regions was consistent with the CFD results. The present study lays a foundation for using the OFV method to directly resolve the velocity fields from the concentration fields of hydrogen jets measured by laser diagnostics.

Keywords: Hydrogen safety; optical flow method; velocity measurements; hydrogen jets

1.0 INTRODUCTION

As a clean energy carrier with many favourable properties, such as renewability, and zero-emission, hydrogen is a promising substitute for conventional fossil fuels to reduce carbon emissions and improve the environment quality. However, hydrogen has to be stored at extremely high pressures for commercial use due to its low volumetric energy density. The hydrogen storage pressures of hydrogen fuel cell vehicles are typically 70 MPa. Risk assessments of the potential leakage accidents at such high pressures are essential for developing safety codes and standards. Concentration and velocity measurements of hydrogen jets are crucial for developing and validating hydrogen jet models. In addition, the hydrogen jets may impact the obstacles which rapidly reduce the initial momentum of the gas jet. The blocked hydrogen flows upward driven by the buoyancy. Concentration and velocity measurements of such low-speed flows contribute to understanding the hydrogen dispersion characteristics and the concentration build-up. Therefore, concentration and

velocity measurements provide scientific bases for hydrogen safety analyses.

The concentration fields can be visualized and accurately measured using laser diagnostics like laser Rayleigh and Raman scattering techniques [1-4]. The current conventional flow field velocimetry methods include the stream filament technique, oil flow method, smoke-wire method [5], hot wire film velocimetry (HWFV) method [6], and laser doppler velocimetry (LDV) method [7], etc. However, these velocimetry methods all have shortcomings differently. The gas filament technique and the oil flow method can only show the trend of the flow with the flow field will be disturbed. The HWFV method contributes to the flow measurement, but it also has great interference in the flow field during the application, and can only measure the velocity at a single point. The smoke visualization method cannot perform quantitative analysis. The laser doppler velocimetry (LDV) method can measure the flow field without contact, but it is still impossible to measure the whole two-dimensional or three-dimensional flow field. Due to the small spatial scale and complex structure of the hydrogen jet, these contact velocimetry methods cannot meet the measurement requirements for the hydrogen jet. With the development of laser diagnosis technology, computer technology, and image processing technology, various non-contact velocimetry technologies that can provide two-dimensional velocity field information has been developed, such as the laser speckle velocimetry (LSV) method [8], particle tracking velocimetry (PTV) method [9] and particle image velocimetry (PIV) method [10-12], etc. The various velocimetry methods mentioned above all belong to the particle image velocimetry method which needs to seeding tracer particles into the flow and then calculates the velocity field by processing the images. Comparing the three methods, the PIV method proving higher measurement accuracy than the LSV method and PTV method.

Particle image velocimetry (PIV) is a kind of non-intrusive transient flow field measurement technology which is commonly used for measuring velocities in turbulent flows by seeding tracer particles into the flow and assuming the particles intimately follow the flow. Tracer particles in the flow are illuminated by a planar laser to produce the particle images at accurate time intervals. The measurement of the particle displacements between two images is the key element for the PIV velocity measurement technology. At present, most of the PIV method obtains the flow field information by the cross-correlation analysis of the particle images [12]. However, the PIV method also has some disadvantages. For example, sometimes the particle seeding is difficult or disturbs the flow field. Besides, the velocity field calculated by the cross-correlation analysis has relatively lower measurement accuracy at the high-velocity gradients region. Moreover, the concentration and velocity measurements are nearly impossible to synchronize when using PIV systems to measure the velocities and other methods to measure the concentrations. It is not conducive to in-depth research on the hydrogen jet.

The optical flow technology originated from computer vision research and was originally used to extract the velocity of rigid body motion, such as the motions of people or cars by processing images with precise time intervals [13-15]. Recently, the optical flow velocimetry (OFV) method has been used for measuring fluid velocity. According to different constraints, the OFV method is divided into various types. The flow field of air jets and Great Red Spot on Jupiter have been quantified by the physics-based optical flow method [16]. The continuous wavelet transforms (CWY) based optical flow has been used to measure the oil leakage underwater and carbon dioxide jets [17, 18]. The HS optical flow method has been used to visualize and quantify the velocity field in a ventilated room [19]. Several studies show that the OFV method can quantify the flow field by processing the concentration field without seeding particles to the flow field, and offer full-field unsteady flow information with potentially high accuracy and resolution. Meanwhile, this method provides a way to measure the concentration and velocity simultaneously. Therefore, the OFV method may offer a potentially simpler and lower-cost way to identify and quantify the fine spatial structures within the hydrogen jet, which is thus effective in the quantitative investigation of shock structure. Before that, the method needs to be verified and the parameters of the method need to be adjusted to make it more suitable for flow field quantification. The computational fluid dynamics (CFD) can be used to verify the OFV method since it is difficult to measure the concentration and velocity simultaneously by

experiments. At the first step, the particle images of hydrogen jets generated by the CFD method are suitable to test the OFV method.

In the present paper, the velocity field and particle images of hydrogen jets were simulated using FLUENT with the large eddy simulation (LES) method, and then the particle images were used to resolve the velocity field by the OFV method. The OFV results were compared with the CFD simulation to verify its accuracy.

2.0 PRINCIPLES OF OPTICAL FLOW METHOD

2.1 optical flow constraint equation

The perspective projection from a fluid medium onto an image is shown in Fig. 1. The movement in three-dimensional space can be transformed into the movement in the two-dimensional image plane by the collinearity equations [20]. The velocity field in the image plane is referred to as the optical flow field. The optical flow is loosely defined as the velocity of the pixels on the image plane. The optical flow vector for each pixel (x, y) constitutes the optical flow field. The optical flow is about the two-dimensional motion of gray value or intensity distributions of a pair of images. The changing intensity is related to the actual physical movement of the object. The velocity distribution in the image can be computed by processing the change of intensity.

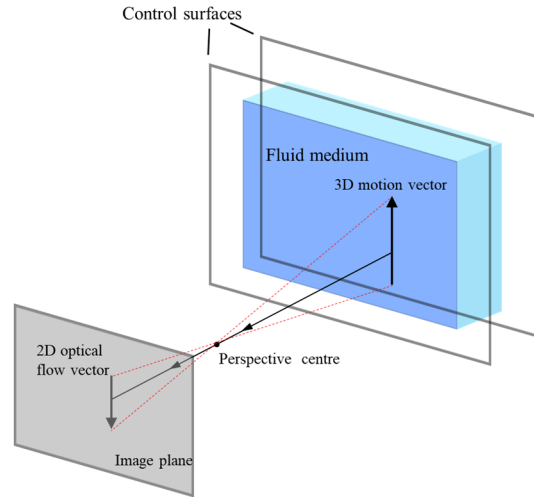


Figure 1. Projection from fluid flow onto the image plane

The basis of the optical flow method is the brightness constancy assumption which assumes that a point keeps the same intensity along its trajectory. The intensity of the pixel (x, y) at the time (t) is denoted as $I(x, y, t)$. According to the brightness constancy assumption, the intensity at the other pixel a little distance away and a little time later is the same as that at the original pixel:

$$I(x + dx, y + dy, t + dt) = I(x, y, t) \quad (1)$$

Substituting the Taylor expansion of the left term into Eq. (1) and neglecting the high order terms yields:

$$I(x, y, t) + \frac{\partial I}{\partial x} dx + \frac{\partial I}{\partial y} dy + \frac{\partial I}{\partial t} dt = I(x, y, t) \quad (2)$$

So:

$$\frac{\partial I}{\partial x} dx + \frac{\partial I}{\partial y} dy + \frac{\partial I}{\partial t} dt = 0 \quad (3)$$

Since dx/dt is the velocity in the x-direction (u) and dy/dt is the velocity in the y-direction (v), the optical flow constraint equation (OFCE) can be written as:

$$I_x u + I_y v + I_t = 0 \quad (4)$$

where I_x , I_y , and I_t are the partial derivative of intensity (I) concerning x , y , and t that can be obtained from the particle images. The deviation between the solution of (u, v) and the conditions required by the optical flow constraint equation can be expressed as:

$$\xi_b = I_x u + I_y v + I_t \quad (5)$$

However, the optical flow vector with two components u and v cannot be estimated by Equation (4) which has only one constraint, and a second constraint is required. The various second constraint resulting in various optical flow methods, such as the Horn-Schunck (HS) algorithm and the Lucas-Kanade (LK) algorithm, which are the typical differential methods.

2.2 HS optical flow

The HS optical flow method introduces smoothness constraints of the global velocity field and assumes that the flow of neighboring pixels should be smooth. The velocity smoothing term can be written as:

$$\xi_c^2 = (\partial u / \partial x)^2 + (\partial u / \partial y)^2 + (\partial v / \partial x)^2 + (\partial v / \partial y)^2 \quad (6)$$

The key ideas of the Horn-Schunck algorithm are to enforce brightness constancy and enforce smooth flow field to compute optical flow. Therefore, the minimization equation can be established by integrating the above two constraints:

$$\xi^2 = \iint (\xi_b^2 + \alpha^2 \xi_c^2) dx dy \quad (7)$$

where the α is a weighting factor to account for noise in the measurement, the ξ_b^2 is the data term, and the ξ_c^2 is the regularization term. Equation (7) can be transformed into:

$$u_{n+1} = u_n - \frac{I_x (I_x u_n + I_y v_n + I_t)}{\alpha^2 + I_x^2 + I_y^2} \quad (8)$$

$$v_{n+1} = v_n - \frac{I_y (I_x u_n + I_y v_n + I_t)}{\alpha^2 + I_x^2 + I_y^2} \quad (9)$$

The velocity vector (u_{n+1}, v_{n+1}) of the $(n+1)$ step can be calculated from the velocity vector (u_n, v_n) of the n step. The equations can be solved by multiple iterations.

2.3 LK optical flow

The Lucas-Kanade optical flow method uses pixels around the target pixel as an image patch ($k \times k$ pixels) and assumes that neighboring pixels have the same displacements. Since all pixels in the image patch satisfy Equation (4), the following equation can be obtained:

$$\begin{bmatrix} I_x(p_1) & I_y(p_1) \\ I_x(p_2) & I_y(p_2) \\ \vdots & \vdots \\ I_x(p_{k \times k}) & I_y(p_{k \times k}) \end{bmatrix} \begin{bmatrix} u \\ v \end{bmatrix} = - \begin{bmatrix} I_t(p_1) \\ I_t(p_2) \\ \vdots \\ I_t(p_{k \times k}) \end{bmatrix} \quad (10)$$

The optical flow field is obtained by the least square method:

$$\begin{bmatrix} u \\ v \end{bmatrix} = \begin{bmatrix} \sum I_x(p_i)I_x(p_i) & \sum I_x(p_i)I_y(p_i) \\ \sum I_y(p_i)I_x(p_i) & \sum I_y(p_i)I_y(p_i) \end{bmatrix}^{-1} \begin{bmatrix} -\sum I_x(p_i)I_t(p_i) \\ -\sum I_y(p_i)I_t(p_i) \end{bmatrix} \quad (11)$$

where the summation is over each pixel in the image patch.

2.4 Error

The total optical flow RMS error in an $m \times n$ pixels image can be quantified by the following equation:

$$\text{Error} = m^{-1}n^{-1} \sum_{i=1}^m \sum_{j=1}^n \sqrt{(u(i,j) - u_{\text{exa}}(i,j))^2 + (v(i,j) - v_{\text{exa}}(i,j))^2} \quad (12)$$

where the subscript “*exa*” denotes the exact velocity distribution.

3.0 NUMERICAL SIMULATION

The CFD method can obtain the particle images, velocity, and concentration fields to evaluate the OFV results. Therefore, the numerical simulation results were used to evaluate the performance of OFV in the present study. The OFV was used to process the particle image pair obtained from the numerical simulation to obtain the velocity field, and the OFV results were then compared with the velocity field of the numerical simulation.

3.1 Geometry and mesh

A free hydrogen jet was modeled using a 2D model as shown in Fig. 2. The computational domain was 55 mm long by 21 mm wide with a 0.5 mm wide inlet located in the middle of the left boundary.

The mesh was generated in ANSYS ICEM with elements concentrated around the inlet to more accurately capture the flow field and hydrogen concentration there. Hexahedral elements were used in the computational domain to improve the mesh quality. The mesh had about 44000 elements, as shown in Fig. 2.

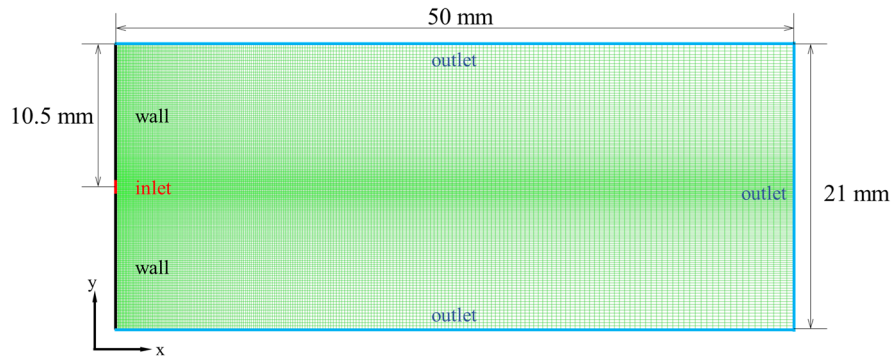


Figure 2. Geometry and mesh

ANSYS Fluent was used for the two-dimensional numerical simulations. The large eddy simulation (LES) model was used for the transient flow calculations. The pressure-based solver has been used with the SIMPLE scheme for the pressure-velocity coupling. The second-order upwind scheme was used for the spatial discretization of density, species, and energy. The second-order interpolation method was used for the pressure and the bounded central differencing was used for the momentum. The influence of gravity and buoyancy on the hydrogen jet were included with the gravitational acceleration ($g=9.81 \text{ m/s}^2$) along the negative X-axis.

The velocity inlet boundary condition (10 m/s) was applied at the hydrogen inlet with the pressure outlet boundary condition ($P=0$ Pa) at the outlet boundary. The walls on both sides of the inlet were set as no-slip stationary walls. The tracer particles were injected into the flow field from the hydrogen inlet by the discrete phase model (DPM). The uniform size particles with $0.1 \mu\text{m}$ diameter were injected into the computational domain from the inlet every 5 time-steps.

4.0 RESULTS AND DISCUSSION

4.1 Vortex pair

A pair of vortices formed at the forefront of the jet. The particle images of the vortex pair at about 22.5 ms after release are shown in Fig. 3 with a 0.01 ms time interval between the two images. The size of the original particle images is 1880×1300 pixels.

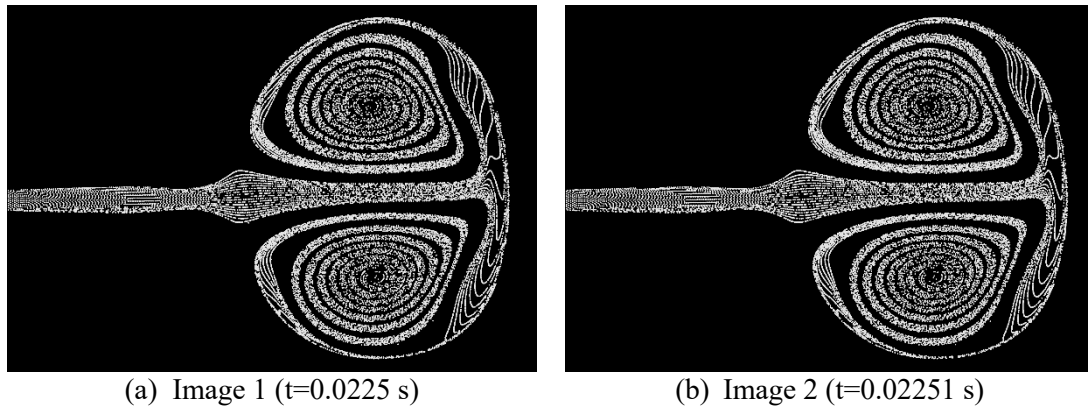


Figure 3. A pair of particle images (1880 pixels by 1300 pixels) with a 0.01 ms interval.

The original images were downsampled by the scale factor (0.5) to ensure the displacements of particles are within a suitable range (1 - 5 pixels) so that the original images are reduced to 50% of the original size. Then, the images were further smoothed by using a Gaussian filter with the 2 -pixel standard deviation to remove the random noise and provide a quasi-continuous intensity field. The preprocessed particle images are shown in Fig. 4.

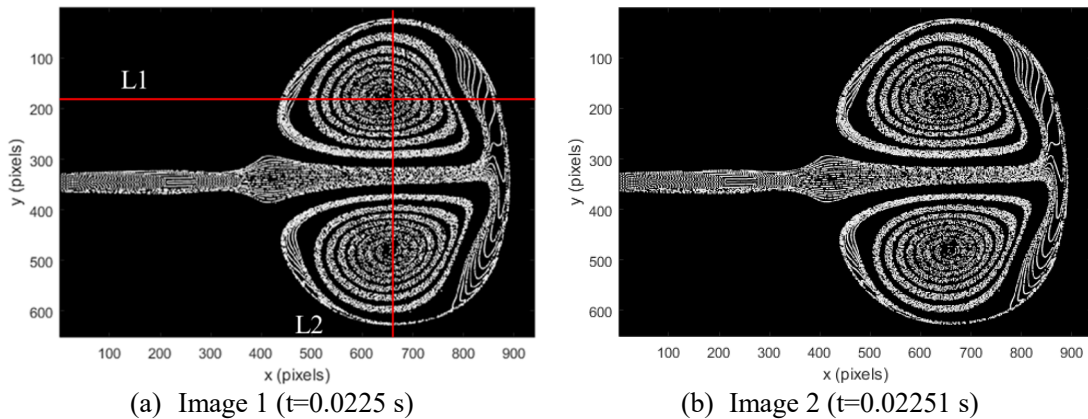


Figure 4. Particle images downsampled by a factor of 0.5 and Gaussian filtered (the 2 -pixel standard deviation) for the initial optical flow computation

The velocity vectors and velocity magnitude contours of the vortex pair extracted from the above particle images using the CFD method and OFV method are shown in Fig. 5 and Fig. 6. The velocity vectors are normalized by their maximum value indicating the direction and relative value in Fig. 5, and the velocity magnitude is indicated by the color of the contours in Fig. 6.

The predicted velocity field by the OFV method was in good agreement with the CFD results especially the area marked with wireframes in Fig. 5 and Fig. 6 where the vortex pair is located. The optical flow method predicted the flow structure and the velocity direction in the regions of high turbulent intensity due to the particle density and displacements at such regions satisfies the application conditions of the optical flow method. However, the velocity field of the mainstream region obtained by the OFV method had a large deviation from the CFD result. The excessively high particle density in the mainstream region caused particles in the optical flow field to overlap each other, which made it difficult to capture the trajectory of particles in the mainstream region.

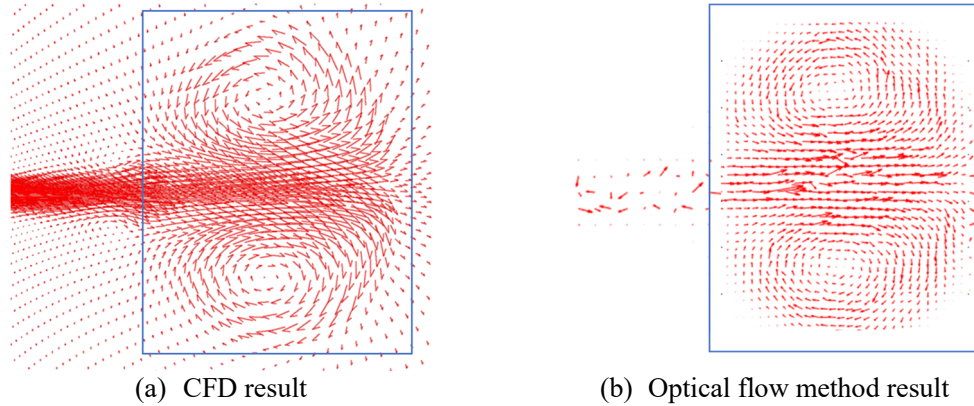


Figure 5. Velocity vectors of a vortex pair in a hydrogen jet extracted from the particle images by using (a) the CFD, and (b) the optical flow method

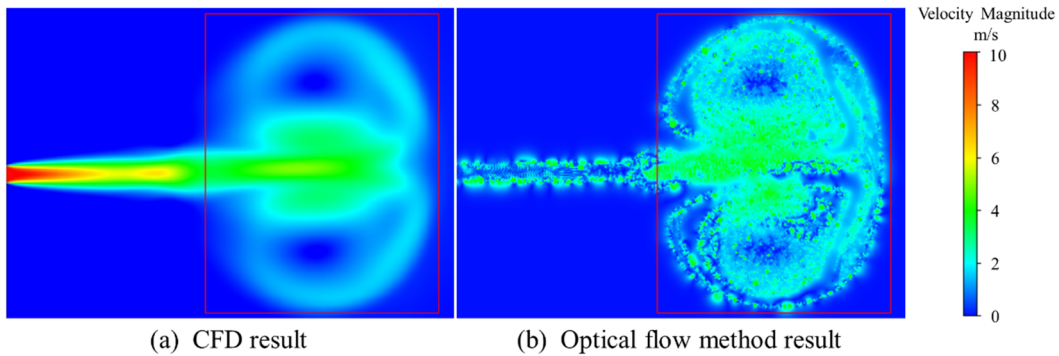
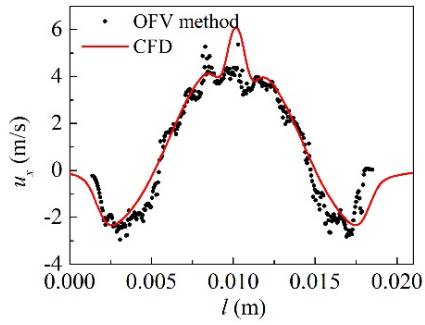


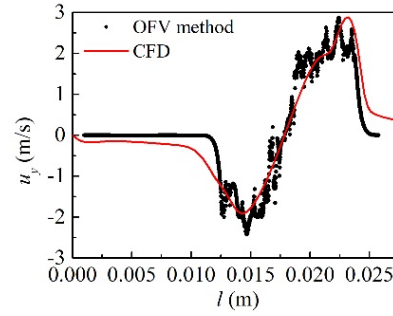
Figure 6. Velocity magnitude contours of a vortex pair in a hydrogen jet extracted from the particle images by using (a) the CFD, and (b) the optical flow method

The result of the optical flow method reflected the velocity distribution of the flow field and was consistent with the CFD result. The OFV method predicted the velocity field by calculating the velocity of each particle. Due to the limited number of particles, the calculated velocity field was discrete. Therefore, the velocity contour by the OFV method was not as smooth as the CFD result. Similarly, the velocity fluctuation in Fig. 7 is also caused by this reason.

The velocity unit given by the optical flow method was pixels/ Δt , where Δt is the interval time between two particle images. The velocity can be converted to m/s by comparing the image size with the actual dimension, which was 1.316×10^{-5} m/pixel in this case. The extracted profiles of the velocity components in x and y directions across the two vortex cores are shown in Fig. 7. Two straight lines, L1 and L2, were across the vortex cores along the x and y directions as illustrated by the red lines in the particle image in Fig. 4(a). The trends in the predicted velocity distributions agree with the CFD results. The optical flow method accurately located the positions of the vortex cores where the velocity is 0. The local error in the OFV method depends on the image intensity gradient [20]. The errors given by Equation (12) were calculated in the whole image, which gave a mean error of 1.1 pixels/unit-time for the OFV method.



(a) The u_x profiles along L2

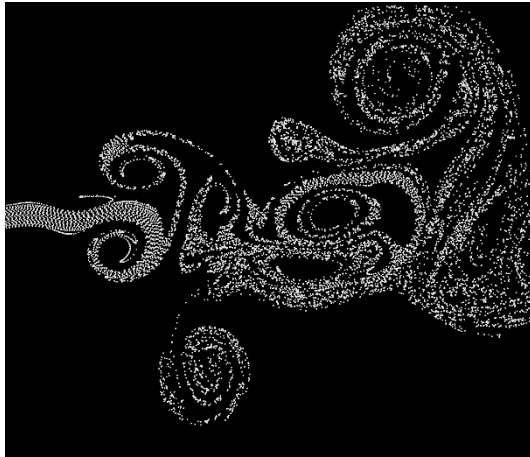


(b) The u_y profiles along L1

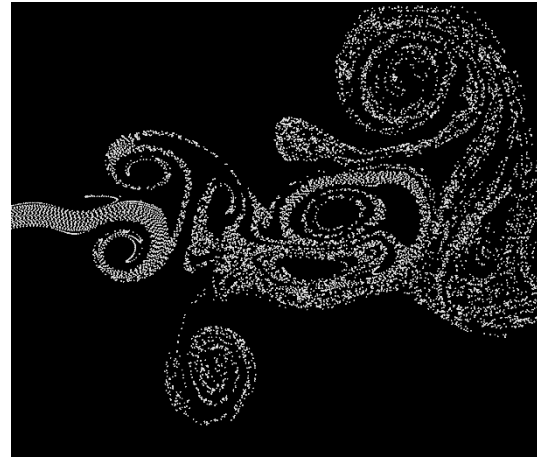
Figure 7. Distribution of the x-component and y-component of velocity across the vortex cores

4.2 Turbulence

The particle images of the flow field at about 0.06 s after release are shown in Fig. 8 with a 0.01 ms time interval between the two images. The original particle images with the size of 1680×1440 pixels were downsampled by the scale factor 0.5 and smoothed by using a Gaussian filter with the 2-pixel standard deviation, as shown in Fig. 9.

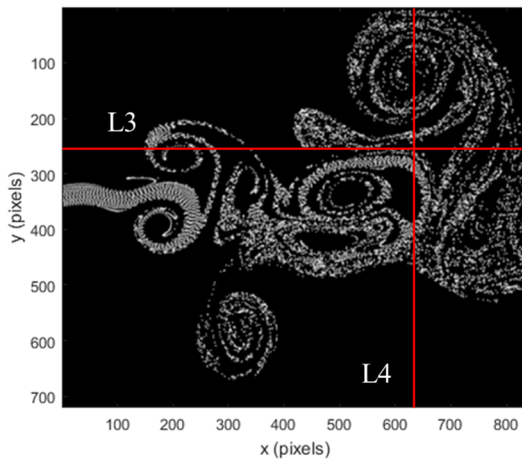


(a) Image 1 ($t=0.06$ s)

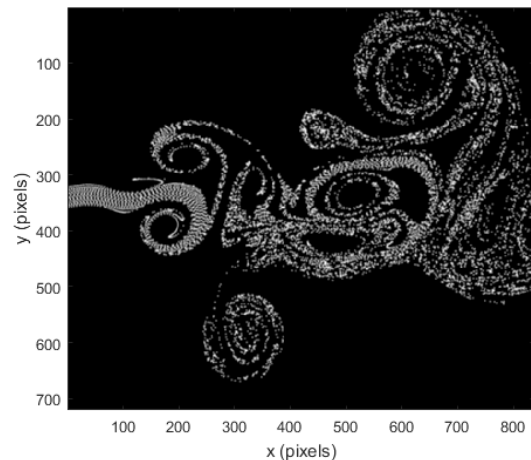


(b) Image 2 ($t=0.06001$ s)

Figure 8. A pair of particle images (1680 pixels by 1440 pixels) with 10 s intervals



(a) Image 1 ($t=0.06$ s)



(b) Image 2 ($t=0.06001$ s)

Figure 9. Particle images downsampled by a factor of 0.5 and Gaussian filtered (the 2-pixel standard deviation) for the initial optical flow computation

The velocity vectors and velocity magnitude contours of the turbulent region of the jet extracted from the particle image pair are shown in Fig. 10 and Fig. 11. The optical flow method accurately located all large vortices which were generated in the shear layer of the free jet due to the Kelvin-Helmholtz instability. Moreover, the velocity field generated by the OFV method had high spatial resolution.

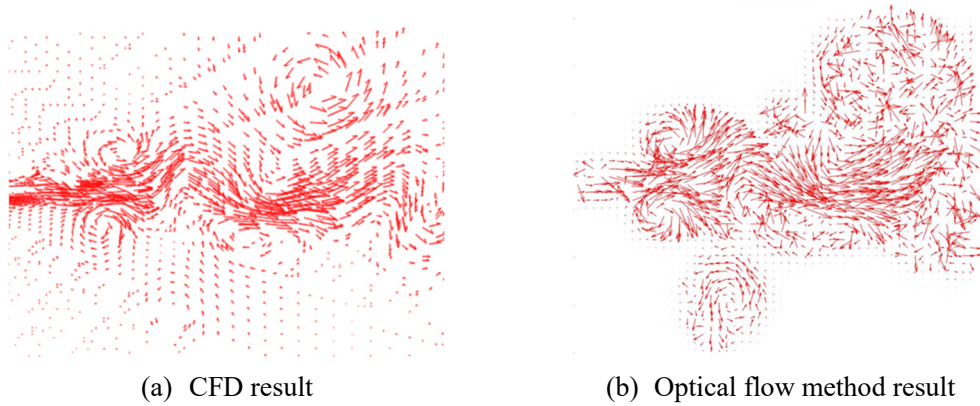


Figure 10. Velocity vectors of the turbulence in a hydrogen jet extracted from the particle images by using (a) the CFD, and (b) the optical flow method

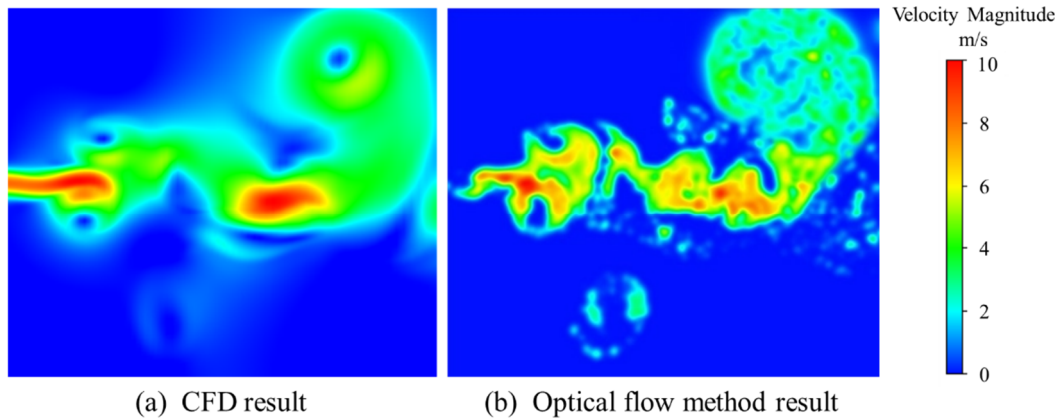


Figure 11. Velocity magnitude contours of the turbulence in a hydrogen jet extracted from the particle images by (a) using the CFD, and (b) the optical flow method

The velocity can be converted to m/s by the factor 1.546×10^{-5} m/pixel in this case. Quantitative comparisons with the CFD results are given in Fig. 12 in the x-velocity and y-velocity profiles along two straight lines L3 and L4. The two lines are illustrated by the red lines on the particle image in Fig. 9(a). The results of the OFV method had similar trends with the CFD results, but the data was not accurate due to the severe fluctuations. This situation may be caused by the mismatch between the parameter setting of the OFV method and the target particle image pair parameters. Therefore, it is necessary to further study the suitable parameters of the OFV method in future work.

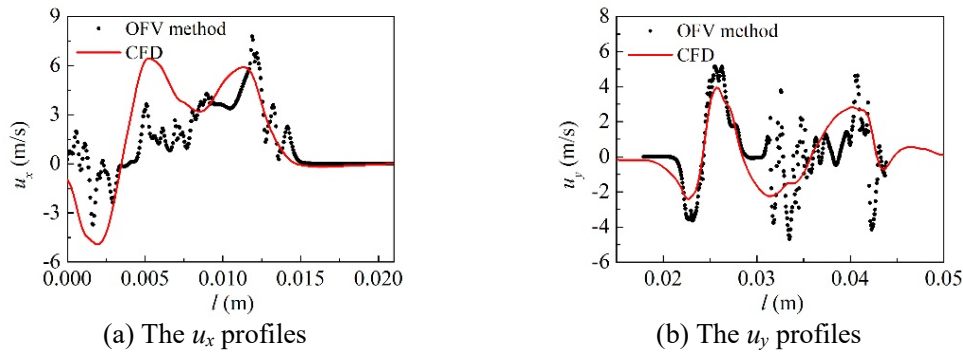


Figure 12. Distribution of the velocity profiles along L3 and L4

5.0 CONCLUSIONS

In the present study, the optical flow velocimetry method was used to resolve the velocity fields from the particle images of hydrogen jets which were generated by the CFD simulations. The OFV results were compared with the CFD simulations, and the results demonstrate that the OFV method is an efficient, low-cost way to extract the velocity fields. The OFV method accurately located the large vortices in the flow field with high spatial resolution. The predicted velocity field obtained by the OFV method agreed with the CFD results except for the mainstream region of the jet where the particle density was too high. The velocity distribution of the high-velocity gradients regions was consistent with the CFD results. The error might be caused by unsuitable parameter settings. The image preprocessing and parameter setting of the OFV method will be further studied in the future, and the concentration contours will be used to obtain the velocity field. The present study lays a foundation for using the OFV method to directly resolve the velocity fields from the concentration fields of hydrogen jets measured by laser diagnostics.

ACKNOWLEDGEMENTS

This study was supported by the National Natural Science Foundation of China (No. 51706125).

REFERENCE

1. Escoda, M.C. and Long, M.B. Rayleigh scattering measurements of the gas concentration field in turbulent jets, *AIAA Journal*, **21**, No. 1, 1983, pp. 81-84.
2. Webber, B.F., Long, M.B. and Chang, R.K., Two-dimensional average concentration measurements in a jet flow by Raman scattering, *Applied Physics Letters*, **35**, No. 2, 1979, pp. 119-121.
3. Li, X.F., Hecht, E.S. and Christopher, D.M., Validation of a reduced-order jet model for subsonic and underexpanded hydrogen jets, *International Journal of Hydrogen Energy*, **41**, 2016, pp. 1348-1358.
4. Ruggles, A.J., Ekoto, I.W., Ignitability and mixing of underexpanded hydrogen jets, *International Journal of Hydrogen Energy*, **37**, No. 22, 2012, pp. 17549–17560.
5. Fukamachi, N., Ohya, Y. and Nakamura, Y., An improvement of the smoke-wire method of flow visualization, *Fluid Dynamics Research*, **7**, No. 1, 1991, pp. 23-29.
6. Sadeghi, M.M., Peterson, R.L. and Najafi, K., Air flow sensing using micro-wire-bonded hair-like hot-wire anemometry, *Journal of Micromechanics & Microengineering*, **23**, No. 8, 2013, pp. 905-923.
7. Quinzani, L.M., Armstrong, R.C. and Brown, R.A., Birefringence and laser-Doppler velocimetry (LDV) studies of viscoelastic flow through a planar contraction, *Journal of Non-Newtonian Fluid Mechanics*, **52**, No. 1, 1994, pp. 1-36.
8. Ma, S. and Lin, Q.Q., Laser speckle velocimetry: using modulated dynamic speckle to measure the velocity of moving diffusers, *Applied Optics*, **25**, No. 1, 1986, pp. 22-25.

9. Maas, H.G., Gruen, A. and Papantoniou, D., Particle tracking velocimetry in three-dimensional flows, *Experiments in Fluids*, **15**, No. 2, 1993, pp. 133-146.
10. Adrian, R.J., Twenty years of particle image velocimetry, *Experiments in Fluids*, **39**, No. 2, 2005, pp. 159-169.
11. Hain, R. and Kähler, C.J., Fundamentals of multiframe particle image velocimetry (PIV), *Experiments in Fluids*, **42**, No. 4, 2007, pp. 575-587.
12. Westerweel, J., Dabiri, D. and Gharib, M., The effect of a discrete window offset on the accuracy of cross-correlation analysis of digital PIV recordings, *Experiments in Fluids*, **23**, No. 1, 1997, pp. 20-28.
13. Horn, B.K. and Schunck, B.G., Determining Optical Flow, Techniques and Applications of Image Understanding. International Society for Optics and Photonics, 12 November 1981.
14. Brox, T., Bruhn, A., Papenbergh, N. and Weickert, J., High Accuracy Optical Flow Estimation Based on a Theory for Warping, Proceeding of the 8th European Conference on Computer Vision, May 2004, Prague, Czech Republic, pp. 25-36.
15. Barron, J.L. and Beauchemin, D., Performance of optical flow techniques, *International Journal of Computer Vision*, **12**, No. 1, 1994, pp. 43-77.
16. Wang, B., Cai, Z.M., Shen, L.X. and Liu, T.S., An analysis of physics-based optical flow, *Journal of Computational and Applied Mathematics*, **276**, 2015, pp. 62-80.
17. Osman, A.B., Ovinis, M., Faye, I., Hashim, F.M. and Osei, H., An Optical Flow Measurement Technique based on Continuous Wavelet Transform, *Journal of Applied Fluid Mechanics*, **11**, No. 3, 2018, pp. 695-707.
18. Schmidt, B.E., Page, W.E. and Sutton, J.A., Seedless Velocimetry in a Turbulent Jet using Schlieren Imaging and a Wavelet-based Optical Flow Method, AIAA, 6-10 January 2020, Orlando.
19. Brecht, A.V., Vranken, E., Guarino, M. and Berckmans, D., Optical flow algorithm to quantify the two-dimensional velocity components of a visualized air jet, *Transactions of the American Society of Agricultural Engineers*, **43**, No. 3, 2004, pp. 847-856.
20. Liu, T.S. and Shen, L.X., Fluid flow and optical flow, *Journal of Fluid Mechanics*, **614**, 2008, pp. 253-291.